



Article

Silicone Elastomer Composites Fabricated with MgO and MgO-Multi-Wall Carbon Nanotubes with Improved Thermal Conductivity

Christopher Kagenda ^{1,2,†} , Jae Wook Lee ^{3,†}, Fida Hussain Memon ^{3,4}, Faheem Ahmed ³, Anupama Samantasinghar ³, Muhammad Wasim Akhtar ^{2,5,*} , Abdul Khaliq ⁵ and Kyung Hyun Choi ^{3,*}

¹ Faculty of Science, Faculty of Chemistry, Chemical Engineering, Kyambogo University, Kampala P.O. Box 1, Uganda; kagztopher@gmail.com

² School of Semiconductor and Chemical Engineering, Chonbuk National University, Jeonju-si 54896, Korea

³ Advanced Micro Mechatronics Laboratory, Department of Mechatronics Engineering, Jeju National University, Jeju-si 63243, Korea; jaewook482@gmail.com (J.W.L.); fida.hussain@iba-suk.edu.pk (F.H.M.); faheemahmedlangah@gmail.com (F.A.); anupamasamantasinghar31@gmail.com (A.S.)

⁴ Department of Electrical Engineering, Sukkur IBA University, Sukkur 65200, Pakistan

⁵ Department of Metallurgy and Materials Engineering, Mehran University of Engineering & Technology, Jamshoro 76062, Pakistan; danialmemon79@gmail.com

* Correspondence: waseem.akhtar@faculty.muuet.edu.pk (M.W.A.); amm@jejunu.ac.kr (K.H.C.)

† Authors contributed equally.



Citation: Kagenda, C.; Lee, J.W.; Memon, F.H.; Ahmed, F.; Samantasinghar, A.; Akhtar, M.W.; Khaliq, A.; Choi, K.H. Silicone Elastomer Composites Fabricated with MgO and MgO-Multi-Wall Carbon Nanotubes with Improved Thermal Conductivity. *Nanomaterials* **2021**, *11*, 3418. <https://doi.org/10.3390/nano11123418>

Academic Editor: Shenmin Zhu

Received: 31 October 2021

Accepted: 10 December 2021

Published: 16 December 2021

Publisher's Note: MDPI stays neutral with regard to jurisdictional claims in published maps and institutional affiliations.



Copyright: © 2021 by the authors. Licensee MDPI, Basel, Switzerland. This article is an open access article distributed under the terms and conditions of the Creative Commons Attribution (CC BY) license (<https://creativecommons.org/licenses/by/4.0/>).

Abstract: The effect of multiwall carbon nanotubes (MWCNTs) and magnesium oxide (MgO) on the thermal conductivity of MWCNTs and MgO-reinforced silicone rubber was studied. The increment of thermal conductivity was found to be linear with respect to increased loading of MgO. In order to improve the thermal transportation of phonons 0.3 wt % and 0.5 wt % of MWCNTs were added as filler to MgO-reinforced silicone rubber. The MWCNTs were functionalized by hydrogen peroxide (H₂O₂) to activate organic groups onto the surface of MWCNTs. These functional groups improved the compatibility and adhesion and act as bridging agents between MWCNTs and silicone elastomer, resulting in the formation of active conductive pathways between MgO and MWCNTs in the silicone elastomer. The surface functionalization was confirmed with XRD and FTIR spectroscopy. Raman spectroscopy confirms the pristine structure of MWCNTs after oxidation with H₂O₂. The thermal conductivity is improved to 1 W/m·K with the addition of 20 vol% with 0.5 wt % of MWCNTs, which is an ~8-fold increment in comparison to neat elastomer. Improved thermal conductive properties of MgO-MWCNTs elastomer composite will be a potential replacement for conventional thermal interface materials.

Keywords: thermal conductivity; silicone elastomer; multi-wall carbon nanotubes

1. Introduction

Due to their light weight, high dimensional accuracy, and adequate properties, polymeric materials have gained significant importance in recent times. Use of polymeric materials has exponentially increased and polymers can extensively be used in fabrication of composite materials. Due to their promising insulating qualities, good thermal stability, high strength, sufficient mechanical properties, biocompatibility, and simplicity in fabrication, elastomers are the second most widely used thermoset polymers after polyester [1–9]. Besides these properties, there are few properties like thermal conductivity that are quite low and do not meet the requirements of many applications. It is important to address these issues to deal with the demand for thermal management applications. The miniaturizing in electronic components makes the heat dissipation problem more significant and drastic. A fractional rise in temperature has consequent effects on the reliability and lifespan of electronic components [10,11]. Thermal interface materials are employed to occupy air

gaps between the assembly when solid parts are joined together. Increase in transportation of phonons by reducing the contact resistance. The reliability and performance of modern electronic devices greatly depend on high thermal conductivity of the thermal interface materials [12].

Polymer nanocomposites are alternatives to conventional thermal interface materials. Thermal grease is often used for thermal interface materials, but it is associated with the 'pump-out' problem; furthermore, the thickness constraint in phase change materials limits its use for heat dissipation applications. Recently, polymer-based thermally conductive composites are typically made by directly combining a polymer matrix with extremely thermally conductive fillers such as carbon black [13], graphene [14,15], boron nitride [16], and alumina [17]; however, the random distribution of fillers in bulk composites typically results in high interfacial thermal resistance and limits the through-plane thermal conductivity in between $1\text{--}5\text{ Wm}^{-1}\text{K}^{-1}$. Modification of filler is one of the probable ways to augment the distribution and interconnective networks among matrix and fillers, thus improving thermal attributes of the composites. The resistance in phonon transportation is curtailed by the formation of strong interfacial connection with filler and matrix by employing functionalization of filler or matrix. Common inorganic fillers—such as alumina, aluminum nitride, and boron nitride—are being employed as thermal conductors for incorporation in polymeric materials [18–20].

Magnesium oxide (MgO) is another filler with attractive characteristics. Bulk thermal conductivity of MgO is far better in comparison to other inorganic fillers. MgO is also widely used in polymer molding as a dielectric powder filler. MgO also possesses a low hardness value compared to other inorganic fillers. The deformation behavior of MgO is similar to metals because of its low hardness [21]. The use of MgO as an effective filler for enhancement of thermal properties of the high viscous elastomers is not extensively studied. Thermal conductivity of MgO/polymer composites has focused on matrices with fewer viscosities like epoxy [22]. However, a higher quantity of MgO filler is essential to enhance thermal properties, since this higher quantity deteriorates mechanical properties. Furthermore, it leads towards the non-homogeneous dispersion of filler which causes interstitial gaps between filler matrix which is an important reason for low conductivity even with a high proportion of MgO filler [23]. As a result, thermally conductive films with relatively low filler loading are preferred. A sufficient thermal conductivity value can even be achieved with low filler loading with good thermal contact. Good interference between particle and matrix decreases the thermal resistance and increases heat dissipation [24].

One possible route to escalate the interference in the filler and matrix is by the addition of functional moieties that generate an effective thermal conductive path between the filler particles and the polymer matrix [2,25,26]. Surface modification helps to generate good interfacial bonds and create an effective thermal bridge for the transportation of phonons [27]. Recently, many reports published that the importance of surface modification is evident in the enhancement of thermal conductivity [2,28–31]. The high aspect ratio and good interface through surface modification are usually key to improve thermal conductivity. Previous reports claim the use of hybrid fillers are effective to enhance thermal conductivity of the composites. [32]. CNTs are intensively used to improve the thermal properties of the composites. The surface modification of CNT with COOH is reported high thermal conductivity [33]. The functional moieties enhance the phonon transportation and thermal conductivity of carbon nanotube fluid as heat transmission channel. The functionalization of CNTs improve the dispersion of the filler in the polymer matrix that counter the agglomeration problem and provide highly thermal conductive path [34]. Another report suggested that the surface modification of graphene with O-phenylenediamine (OPD) aids in augmenting the thermal conductivity of the composite. An increment of 13-fold in in-plane and 4-fold in through-plane thermal conductivity was recorded after the functionalization of graphene [35]. However, the use of a single thermal conductive filler is not that effective and requires a large proportion to achieve adequate thermal conductive characteristics. The use of multi-structured hybrid filler

is advantageous to utilize the properties of various fillers which are not possible in the case of single thermal conductive filler [36]. Hetero-structured fillers have highly thermal conductive networks that provide resistance-free transportation of phonons and synergistic improvement in thermal properties [37,38].

Herein, we report a novel approach by incorporating MgO and MWCNT in the matrix of silicon rubber (KE-12). The surface oxidation of MWCNT incorporates oxygen-containing functional groups onto the graphitic surface of CNTs enhances interfacial adhesion as well as establishing a bond with MgO. Furthermore, the high aspect ratio of CNTs helps in generation efficient thermal conductive networks in hybrid structure that decreases the Kapitza resistance and improves phonon transportation, resulting in improved thermal conductivity of the composite that can be used as potential thermal interface materials (TIMs).

2. Experimental Methods

2.1. Materials

MWCNTs of high purity were acquired from NanoTech Co. Ltd., Jeonju, South Korea with external diameters of 8–15 nm, inside diameters of 3–5 nm, and lengths of 10–50 μm . Sodium hydroxide (NaOH) and magnesium chloride ($\text{MgCl}_2 \cdot 6\text{H}_2\text{O}$) were bought from Samchun chemicals Co. Ltd., Jeonju, South Korea. Urea and Ethanol were obtained from DaeJung Chemicals, Jeonju, South Korea. 30% H_2O_2 was purchased from Junsei Chemical Co. Ltd., Japan. The RTV silicon rubber KE-12 and its hardener were obtained from Shin-Etsu, Japan. All chemical reagents used in this experiment were of analytical grade and used as received.

2.2. Synthesis of MgO

Synthesis of nanoscale MgO was done by mixing 8 g of NaOH with 25 mL of deionized water. Besides, MgCl_2 solution of (4.0 M) was further added within span of 10 min. Later prepared mixture of solution was stirred using a mechanical stirrer at 60 $^\circ\text{C}$ for 1 h. Obtained solution was subsequently aged for 10 h at 60 $^\circ\text{C}$. Synthesized precipitates of MgO were rinsed in ethanol and vacuum dried at 60 $^\circ\text{C}$, with subsequent calcination at 150 $^\circ\text{C}$ for 2 h.

2.3. Preparation of H_2O_2 Surface Modified MWCNTs

0.5 g in 30% H_2O_2 of 10 mL MWCNTs were oxidized through stirring for 24 h at the temperature of 65 $^\circ\text{C}$ as reported [39]. The oxidized MWCNTs were washed with de-ionized water, using filter paper of 0.45 μm Millipore membrane. The filtrate was dried overnight at the temperature of 110 $^\circ\text{C}$, later vacuum-dried for 6 h at the temperature of 150 $^\circ\text{C}$ to expel adsorbed H_2O_2 and coupled peroxide functional groups from the surface of the MWCNTs.

2.4. Fabrication of Filler/Silicone Elastomer Composites

The same procedure was followed in the fabrication of filler/silicone elastomer composites of MgO and MgO-MWCNTS composites. In MgO/silicone elastomer composites, the filler loading into the elastomer matrix varied from 10 to 40 vol% while in MgO-MWCNTs hybrid/silicone elastomer composite, the MgO loading was maintained at 20 vol% and the amount MWCNTs added were 0.3 and 0.5 vol% to each loading of MgO. In a typical procedure, after the contents were measured in the required amount, they were mixed with the measured amount of silicone resins using a high-speed Thinky mixer at the speed of 1500 RPM for 15 min. Later, hardener was added to the mixture, which was subsequently casted into furnished molds, followed by curing at ambient temperature for 48 h.

3. Results and Discussion

3.1. Macroscopic and Structural Evolution MgO Nanoparticles

The surface topography of the prepared $\text{Mg}(\text{OH})_2$ and MgO nanoparticles was done through FE-SEM and TEM as shown in Figure 1a–d. It is evident from SEM and TEM that the particle size of $\text{Mg}(\text{OH})_2$ and MgO nanoparticles lies in the range of 50–70 nm before and after calcination as shown in Figure 1. It is observed from the surface morphology of MgO nanoparticles that the basic hexagonal crystalline template of MgO is almost retained after calcination. This insignificant contrast demonstrates that calcination has little effect on the morphology of the nanoparticles. The agglomeration in the particles is due to the presence of the surfactant that was already reported elsewhere [40].

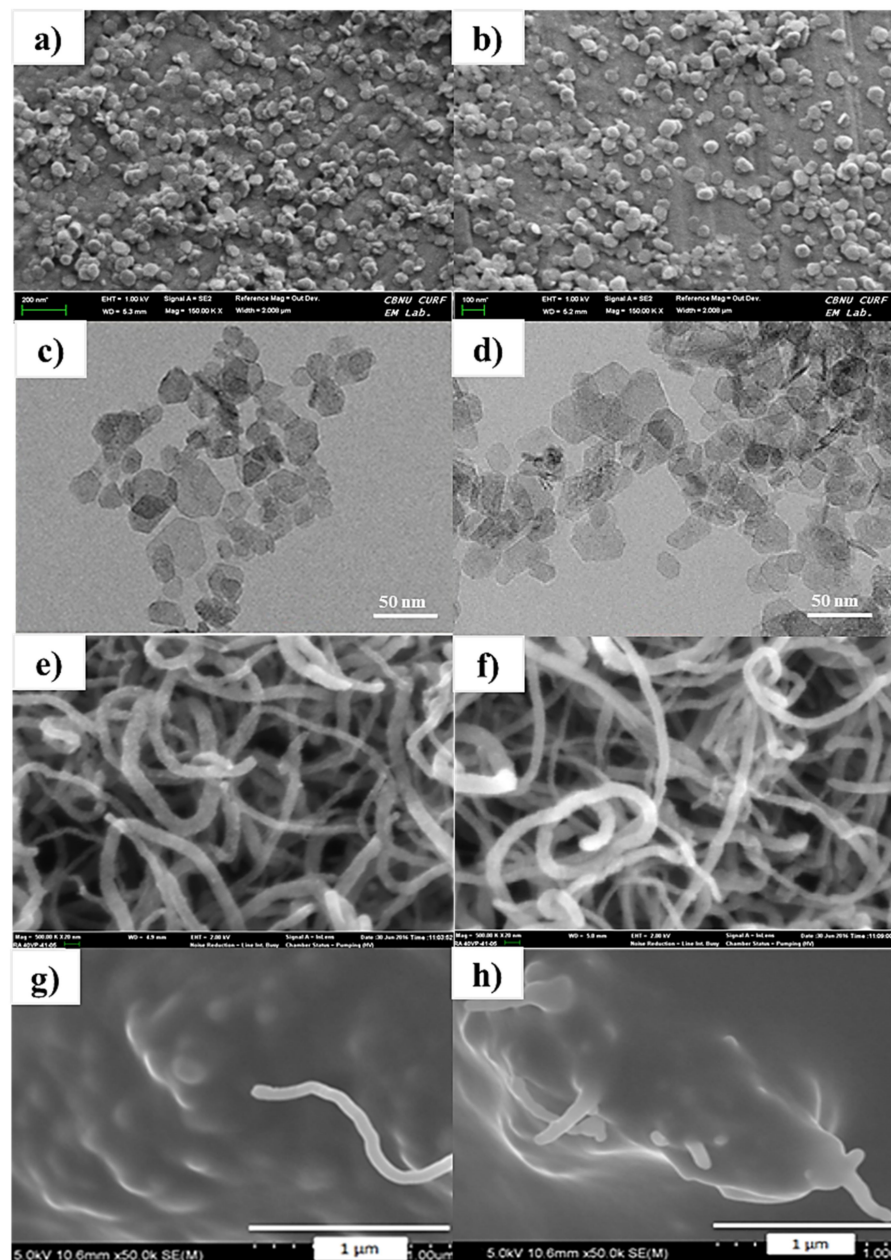


Figure 1. FE-SEM images of (a) $\text{Mg}(\text{OH})_2$ and (b) MgO; HR-TEM images of urea assisted (planet-like) (c) $\text{Mg}(\text{OH})_2$ and (d) MgO, morphology of MWCNTs; FESEM image of (e) controlled MWCNTs; (f) H_2O_2 treated MWCNTs, FE-SEM images of cross-section of MgO-MWCNT/silicone resins composites; (g) 20 vol%–0.5 vol% H_2O_2 -MWCNTs MWCNTs; (h) 30 vol%–0.5 vol% H_2O_2 -MWCNTs.

The crystallinity of $\text{Mg}(\text{OH})_2$ and MgO was characterized using the XRD spectroscopy as in Figure 2. In Figure 2a, the diffraction lines confirm with the JCPDS card analyzer for $\text{Mg}(\text{OH})_2$. The XRD spectra of MgO calcined at 450°C . The presence of peaks at 2θ values of 36.9° , 42.9° , 62.3° , and 74.6° and 78.6° can be indexed to the (1 1 1), (2 0 0), (2 2 0), (3 1 1), and (2 2 2) planes of the face-centered cubic (FCC) structured MgO nanoparticle. The absence of other peaks in the XRD spectra confirms the high crystallinity and purity of MgO nanoparticles (JCPDS file no. 98-17-0905) as shown in (Figure 2b). Average crystallite size was obtained in range of 60 nm, that was calculated using Scherrer's Equation.

$$D = \frac{K \lambda}{\beta \cos \Theta}$$

- D = Mean size of the ordered (crystalline) domains;
- K = Constant;
- λ = X-ray wavelength;
- β = Line broadening at half the maximum intensity (FWHM);
- Θ = Peak position

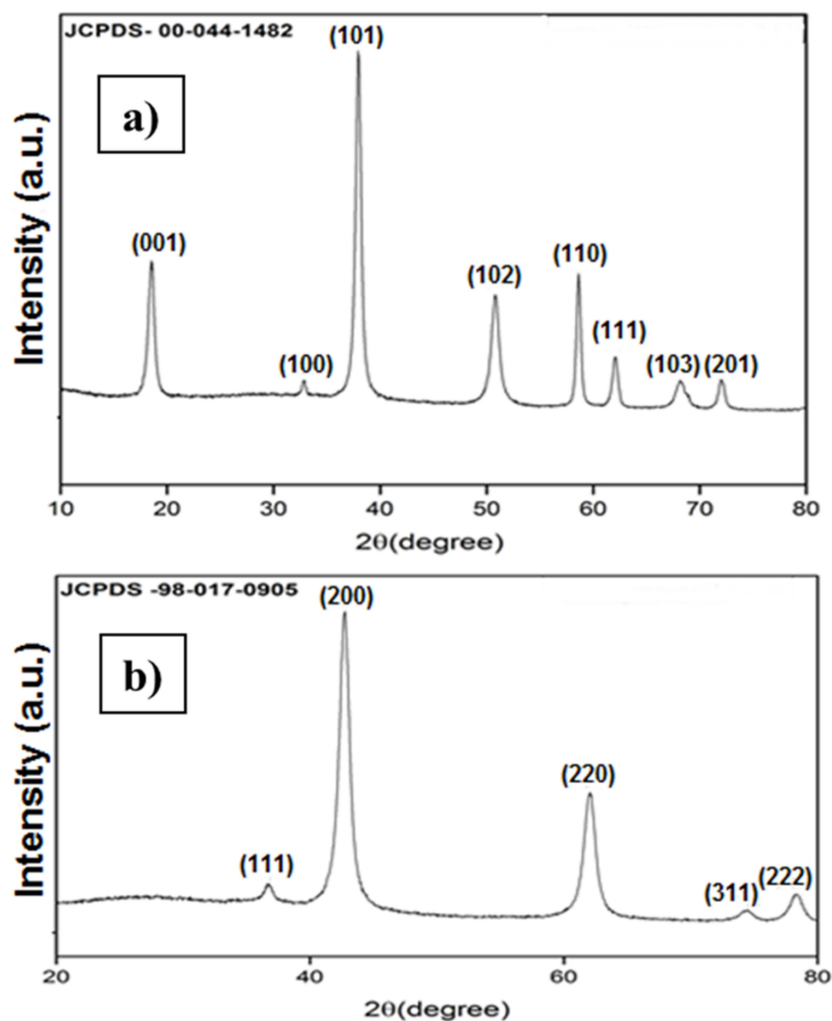


Figure 2. XRD patterns of (a) $\text{Mg}(\text{OH})_2$ and (b) MgO .

3.2. Surface Treatment of Multi-Walled Carbon Nanotubes (MWCNTs)

The surface modification of MWCNT was studied by FTIR spectroscopy. In the pristine MWCNTs spectrum (Figure 3a), pristine MWCNT samples show strong peak

around 1632 cm^{-1} attributed to C=C stretching mode. The peak at 1037 cm^{-1} is due to stretching mode of C-O (COH). The peak at 2919 cm^{-1} is due to the asymmetric C-H_n and symmetric C-H_n stretching mode. The peak at around 3446 cm^{-1} corresponding to OH peak is related to absorbed water molecules on the carbon in the MWCNTs. The results are in good agreement with previously reported literature [41]. H₂O₂-treated MWCNTs at 12 h showed the same effect on band peaks as the pristine MWCNTs showed and no oxidation was observed within 12 h of treatment (Figure 3b). However, as the oxidation time is increased, the spectrum (Figure 3c,d) of the oxidized sample shows, the -COOH, -C=O, and -OH band peaks prominently declined. A new peak at 1727 cm^{-1} is appeared due to C=O stretching frequency, that shows the presence of carboxylic group, formed during the oxidation of MWCNTs. After 48 h, the intensity of C=O implies more number of carboxylic groups attached to MWCNTs due to further oxidation. Furthermore, two new peaks are also observed at around 2936 and 2847 cm^{-1} belonging to CH₂ group on the surface of H₂O₂-MWCNT-48 CH shows the higher stability of oxidized MWCNTs in comparison to pristine MWCNTs [42].

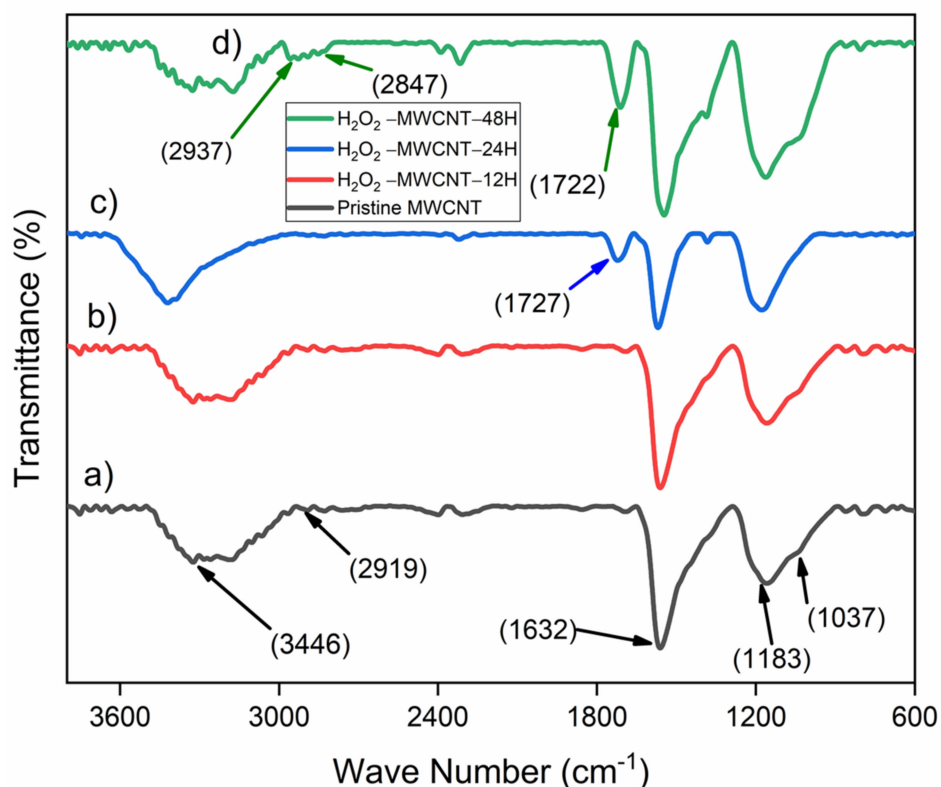


Figure 3. FTIR spectra of MWCNTs and H₂O₂-treated MWCNTs. (a) Pristine MWCNTs; (b) H₂O₂-MWCNTs for 12 h; (c) H₂O₂-MWCNTs for 24 h; and (d) H₂O₂-MWCNTs for 48 h.

The Raman spectrum was observed from the MWCNTs (CO-based) at ambient temperature as in Figure 4. Raman spectra exhibits two Raman peaks, namely G(graphite)- and D(disorder)- the band of MWCNTs. The peak at around 1580 cm^{-1} because of the Raman-active E_{2g} mode analogous to that of graphite [43,44], and the D-peak is because of the breathing modes of the sp^2 atoms, providing the defects at the first Brillouin zone [45]. The I_G/I_D ratio of the neat MWCNT specimen was 0.86. It is a common indicator of a significant number of structural flaws in MWCNT graphitic structure. Such a structure provides many active sites for more modification as reported [39]. It can also be observed from (Figure 4a) that the vibrational properties of the MWCNT altered the I_G/I_D ratio to 0.85, 0.82, and 0.80 for 12-, 24-, and 48-h treatment with H₂O₂ respectively. This I_G/I_D ratio change in the oxidized material has been reported before. It has been associated with the inception of latest defects, and geometrical alterations in MWCNT [39,46–48]. More similar

observations include the D-band region upshifts in the oxidized sample. The increment of the D peak can be observed which confirms the attachment of functional moieties on the surface of MWCNTs Figure 4b.

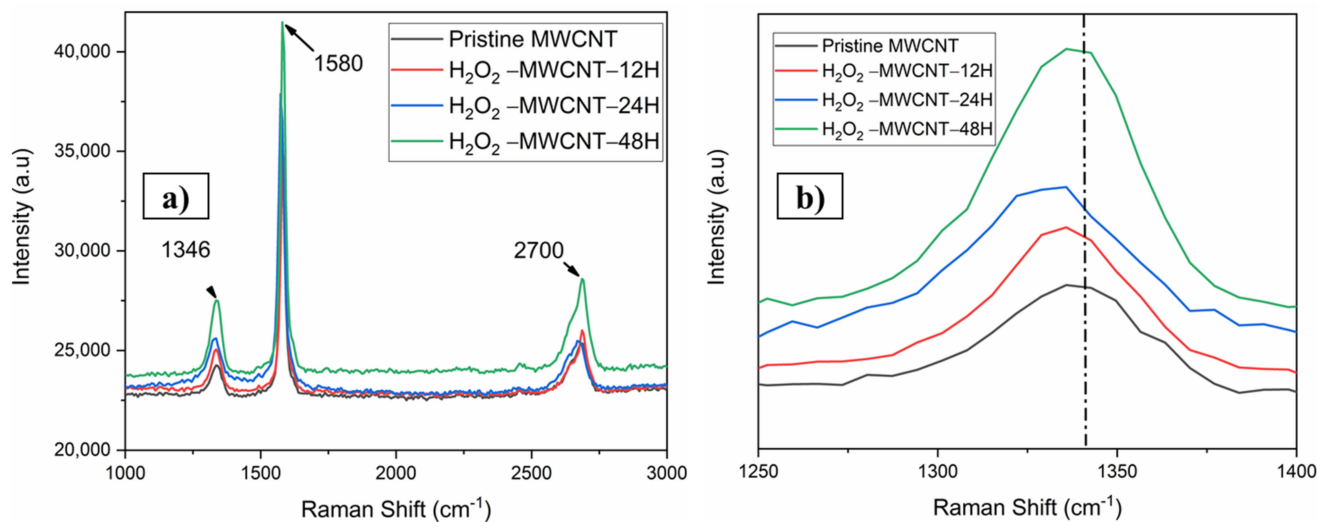


Figure 4. (a) Raman spectra of pristine MWCNTs and H₂O₂ treated MWCNTs, and (b) magnified spectra of D peak.

FESEM images of pristine MWCNTs and the oxidized MWCNTs (24 h) as shown in Figure 1e,f. The graphitic structure of pristine MWCNTs was very smooth and highly visible in comparison to oxidized MWCNTs (Figure 1e). After oxidation, the MWCNTs bundles appear exfoliated and twisted, it is due to erosion during the oxidation of MWCNTs with H₂O₂ as shown in (Figure 1f). The oxidizing agent causes extreme etching on graphitic surface of MWCNTs. This observation rhymes well with the afore-mentioned outcomes of Raman spectroscopy are based on preferential oxidation at defect sites and disintegration of nanotubes. Nevertheless, the wall structures of the MWCNTs were partially eroded by oxidation within 24 h; however, rest of the fragments possessed better graphitic structure [49].

3.3. Thermal Conductivity of MgO-Filled Silicone Rubber

Thermal conductivity of elastomer composite was carried out with advance laser flash operating system (NETZSCH LFA 457 MicroFlash Jeonju, South Korea). Equipped with an infrared detector on top LFA is a contact-less transient thermal analysis technique, extensively utilized for a broad variety of materials ranging between 0.01 mm²/s to 1000 mm²/s. It works with combination of latest technology with state-of-the-art data analyzing methods, that are completely automated techniques where optimal signal-to-noise ratio is achieved. Both finite pulse effect and heat loss are taken into consideration for processing of acquired data in this technique [50]. This LFA technique has a clear advantage over hot disk method and transient plane-source (TPS) thermal conductivity analyzing techniques. Having discrepancies between heat transfer process and data analysis used by idealized models, the hot disk and transient plane-source TPS methods suffer considerable systematic flaws when applied to lower thermal conductivity/thermal insulation materials [51]. Thermal conductivity is shown in Figure 5 for different loading of MgO and MgO-MWCNT into silicone elastomer. The thermal conductivity of pristine silicone elastomer is 0.2 W/m·K whereas, that of MgO/silicone elastomer composites increases along MgO content loading. The highest total MgO filler content considered in this work was 30 vol% because higher percentages are known to compromise rheological control [22]. The MgO-incorporated silicone rubber exhibits greater thermal conductivity due to greater intrinsic thermal conductivity (Figure 5a). Although, at a lower concentration, the stuffed silicone rubber demonstrates relatively low thermal conductivity as compared to what is

expected, probably due to the failure of the nanoparticles to develop perfect thermally conductive pathways lower than 10 vol% loading. However, the nanoparticles, the superfine size, and greater surface energy enable them to become hard to scatter uniformly in silicone rubber. Consequently, most of the nanoparticles get disintegrated through silicon rubber and are unable to produce conductive pathways in the matrix. At 20 vol% concentration or above, nanoparticles started to develop a dense structure inside the matrix, that is more firm and thicker that provides heat conductive pathways due to huge volume proportion of nanoparticles at identical mass fraction. It can be seen, from FE-SEM micrographs, that the nano-sized MgO particles are not distributed uniformly in the elastomer matrix as in Figure 1g,h. However, with an increase in filler loading, MgO nanoparticles contact more. The condition of filler diffusion is crucial, filler units must be cohesive to develop a continuous heat conduction path and increase the thermal properties positively [52]. However, the composite shows greater thermal conductivity. The thermal conductivity is enhanced 40-fold (1.032 W/m·K) in comparison to neat elastomer with the addition of 30 vol% MgO loading filled with 0.5 vol% H₂O₂-MWCNTs (Figure 5b). The application of MWCNTs inter-connective paths between MgO and the matrix. FESEM analysis of the composites displayed a non-homogenous distribution at higher loading of MWCNTs Figure 1g,h. On the other hand, the existence of interfacial associations among the nanotubes, MgO, and the matrix is important in creating thermal conductive pathways, is not obvious. The higher increase of thermal conductivity of H₂O₂-MWCNTs compared to pristine MWCNTs is due to the functionalization that provides activation of organic groups at the MWCNTs surface [53]. In the course of processing, carbon nanotubes were properly distributed in the composite with low MgO percentage loading—i.e., 10 and 20 vol%—but re-agglomerated after incorporation with higher loading thus being entrapped between elastomer molecules. Subsequently, a separation between the CNTs and MgO ensues due to inhomogeneous mixing. This separation inhibits heat flow from particle to particle, leading to the rapid decrease of thermal conductivity at filler loading with 30 vol% MgO [54]. The thermal conductivity of 20 vol% hybrid composite with 0.5 vol% H₂O₂-MWCNTs content is 1.006 W/m·K which is a 44% increase paralleled to the 31% increase in MgO/pristine MWCNTs (0.918 W/m·K). Composites with H₂O₂ treated MWCNTs show higher thermal conductivity than those with pristine MWCNTs because the MWCNT surfaces are altered; creating good cohesion between filler and silicone resins matrix in composites will be signified (Figure 5b). Better adhesion between filler and polymer matrix can decrease the thermal blockade of the interface of filler and matrix [54].

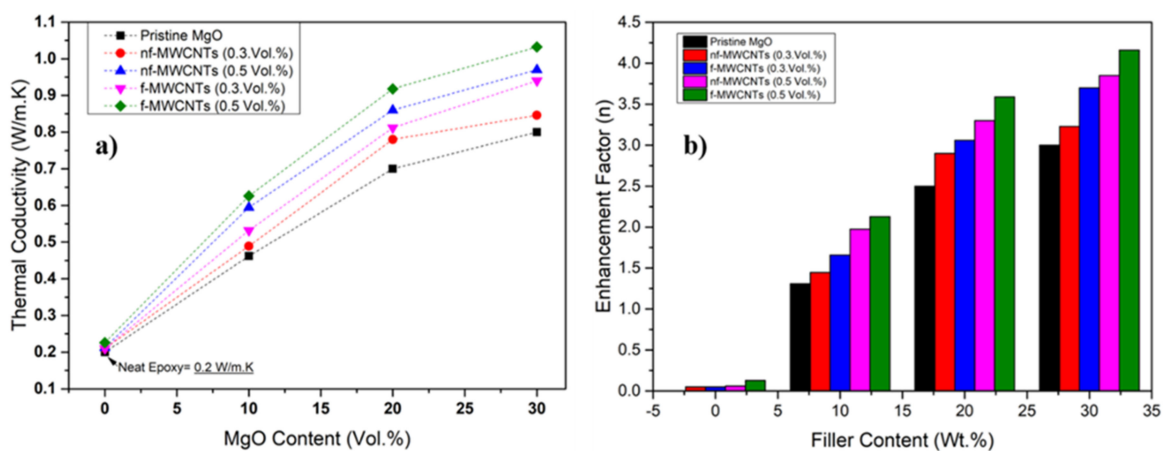


Figure 5. (a) Thermal conductivity of MgO/P-MWCNTs and MgO/H₂O₂-MWCNTs/silicone elastomer composites; (b) Enhancement in thermal conductivity as a function of filler content.

4. Conclusions

This work presents a simple method to increase the thermal conductivity of silicone elastomer by using a low amount of high-aspect-ratio MWCNTs in MgO-filled silicone rubber in an attempt to find a suitable and convenient method for industrial application. The thermal conductivity is linearly increased with the addition of MgO nanoparticles. For improving the heat transfer in composites between the matrix and fillers, the high-aspect-ratio MWCNTs were incorporated in the elastomer matrix after functionalization with H₂O₂. Functionalized MWCNTs were used as source material before their incorporation into the MgO polymer matrix. The functional group residues suggest the effects of particle dispersion on the nanotubes in the matrix at various MgO loading. The thermal conductivity is enhanced 40-fold (1.032 W/m·K) in comparison to neat elastomer with the addition of 30 vol% MgO loading filled with 0.5 vol% H₂O₂-MWCNTs. The developed composite with low filler content will be appropriate for heat dissipation applications.

Author Contributions: Conceptualization, C.K. and J.W.L.; methodology, C.K. and F.H.M.; software, F.A.; validation, A.S., C.K. and A.K.; formal analysis, F.H.M. and F.A.; investigation, M.W.A., A.S. and A.K.; resources, K.H.C. and M.W.A.; data curation, A.K. and F.H.M.; writing—original draft preparation, C.K. and J.W.L. and A.K.; writing—review and editing, K.H.C. and M.W.A.; visualization, A.K.; supervision, K.H.C.; project administration, K.H.C. and M.W.A.; funding acquisition, K.H.C. All authors have read and agreed to the published version of the manuscript.

Funding: This work was supported by the innovation lab support program for material, parts, equipment (20012558, Commercialization of nanocarbon composites in sensor and biomedical industries) funded by the Ministry of Trade, Industry, and Energy (MOTIE, Korea).

Institutional Review Board Statement: Not Applicable.

Informed Consent Statement: Not Applicable.

Data Availability Statement: Not Applicable.

Conflicts of Interest: The authors declare no conflict of interest.

References

1. Ueta, G.; Wada, J.; Okabe, S.; Miyashita, M.; Nishida, C.; Kamei, M. Insulation characteristics of epoxy insulator with internal delamination-shaped micro-defects. *IEEE Trans. Dielectr. Electr. Insul.* **2013**, *20*, 1851–1858. [CrossRef]
2. Akhtar, M.W.; Kim, J.S.; Memon, M.A.; Baloch, M.M. Hybridization of hexagonal boron nitride nanosheets and multilayer graphene: Enhanced thermal properties of epoxy composites. *Compos. Sci. Technol.* **2020**, *195*, 108183. [CrossRef]
3. Yamini, S.; Young, R.J. The mechanical properties of epoxy resins. *J. Mater. Sci.* **1980**, *15*, 1823–1831. [CrossRef]
4. Mughal, M.M.; Akhtar, M.W.; Baloch, M.M.; Memon, M.A.; Syed, J.A.; Kim, J.S. Effect of silanized sisal fiber on thermo-mechanical properties of reinforced epoxy composites. *J. Compos. Mater.* **2019**, *54*, 2037–2050. [CrossRef]
5. Xie, M.; Wang, Z. Synthesis and Properties of a Novel Cycloaliphatic Epoxide. *Macromol. Rapid Commun.* **2001**, *22*, 620–623. [CrossRef]
6. Asif, A.; Kim, K.H.; Jabbar, F.; Kim, S.; Choi, K.H. Real-time sensors for live monitoring of disease and drug analysis in microfluidic model of proximal tubule. *Microfluid. Nanofluid.* **2020**, *24*, 43. [CrossRef]
7. Asif, A.; Park, S.H.; Soomro, A.M.; Khalid, M.A.U.; Salih, A.R.C.; Kang, B.; Ahmed, F.; Kim, K.H.; Choi, K.H. Microphysiological system with continuous analysis of albumin for hepatotoxicity modeling and drug screening. *J. Ind. Eng. Chem.* **2021**, *98*, 318–326. [CrossRef]
8. Salih, A.R.C.; Hyun, K.; Asif, A.; Soomro, A.M.; Farooqi, H.M.U.; Kim, Y.S.; Kim, K.H.; Lee, J.W.; Huh, D.; Choi, K.H. Extracellular Matrix Optimization for Enhanced Physiological Relevance in Hepatic Tissue-Chips. *Polymers* **2021**, *13*, 3016. [CrossRef]
9. Zhang, Y.; Ruan, K.; Gu, J. Flexible Sandwich-Structured Electromagnetic Interference Shielding Nanocomposite Films with Excellent Thermal Conductivities. *Small* **2021**, *17*, 2101951.
10. Yu, A.; Ramesh, P.; Itkis, M.E.; Bekyarova, E.; Haddon, R.C. Graphite Nanoplatelet–Epoxy Composite Thermal Interface Materials. *J. Phys. Chem. C* **2007**, *111*, 7565–7569. [CrossRef]
11. Viswanath, R.; Wakharkar, V.; Watwe, A.; Lebonheur, V.; Manufacturing Group; Intel Corp. Thermal Performance Challenges from Silicon to Systems. 2000. Available online: <http://citeseerx.ist.psu.edu/viewdoc/summary?doi=10.1.1.14.8322> (accessed on 1 October 2021).
12. Chandran, A.M.; Varun, S.; Mural, P.K.S. Comparative study on thermal and electrical transport properties of hexagonal boron nitride and reduced graphene oxide/epoxy nanocomposite by transient plane source techniques and impedance spectroscopy. *J. Mater. Sci. Mater. Electron.* **2021**, *32*, 25350–25362. [CrossRef]

13. Li, Y.; Wang, S.; Zhang, Y.; Zhang, Y. Carbon black-filled immiscible polypropylene/epoxy blends. *J. Appl. Polym. Sci.* **2006**, *99*, 461–471. [[CrossRef](#)]
14. Shahil, K.M.; Balandin, A. Thermal properties of graphene and multilayer graphene: Applications in thermal interface materials. *Solid State Commun.* **2012**, *152*, 1331–1340. [[CrossRef](#)]
15. Khan, J.; Ullah, H.; Sajjad, M.; Bahadar, A.; Bhatti, Z.; Soomro, F.; Memon, F.H.; Iqbal, M.; Rehman, F.; Thebo, K.H. High yield synthesis of transition metal fluorides (COF₂, NiF₂, and NH₄MnF₃) nanoparticles with excellent electrochemical performance. *Inorg. Chem. Commun.* **2021**, *130*, 108751. [[CrossRef](#)]
16. Yu, C.; Zhang, J.; Li, Z.; Tian, W.; Wang, L.; Luo, J.; Li, Q.; Fan, X.; Yao, Y. Enhanced through-plane thermal conductivity of boron nitride/epoxy composites. *Compos. Part A Appl. Sci. Manuf.* **2017**, *98*, 25–31. [[CrossRef](#)]
17. McGrath, L.M.; Parnas, R.S.; King, S.H.; Schroeder, J.L.; Fischer, D.A.; Lenhart, J.L. Investigation of the thermal, mechanical, and fracture properties of alumina–epoxy composites. *Polymers* **2008**, *49*, 999–1014. [[CrossRef](#)]
18. Choi, S.; Kim, J. Thermal conductivity of epoxy composites with a binary-particle system of aluminum oxide and aluminum nitride fillers. *Compos. Part B Eng.* **2013**, *51*, 140–147. [[CrossRef](#)]
19. Xu, Y.; Chung, D.; Mroz, C. Thermally conducting aluminum nitride polymer-matrix composites. *Compos. Part A Appl. Sci. Manuf.* **2001**, *32*, 1749–1757. [[CrossRef](#)]
20. Cheewawuttipong, W.; Fuoka, D.; Tanoue, S.; Uematsu, H.; Iemoto, Y. Thermal and Mechanical Properties of Polypropylene/Boron Nitride Composites. *Energy Procedia* **2013**, *34*, 808–817. [[CrossRef](#)]
21. Ishigaki, H.; Buckley, D.H. Effects of Environment on Microhardness of Magnesium Oxide. 1982. Available online: <https://ntrs.nasa.gov/citations/19820014492> (accessed on 1 October 2021).
22. Wereszczak, A.A.; Morrissey, T.G.; Volante, C.N.; Farris, P.J.; Groele, R.J.; Wiles, R.H.; Wang, H. Thermally conductive MgO-filled epoxy molding compounds. *IEEE Trans. Compon. Packag. Manuf. Tech.* **2013**, *3*, 1994–2005. [[CrossRef](#)]
23. Zhou, W.; Wang, C.; An, Q.; Ou, H. Thermal Properties of Heat Conductive Silicone Rubber Filled with Hybrid Fillers. *J. Compos. Mater.* **2008**, *42*, 173–187. [[CrossRef](#)]
24. Ruan, K.; Guo, Y.; Lu, C.; Shi, X.; Ma, T.; Zhang, Y.; Kong, J.; Gu, J. Significant Reduction of Interfacial Thermal Resistance and Phonon Scattering in Graphene/Polyimide Thermally Conductive Composite Films for Thermal Management. *Research* **2021**, *2021*, 8438614. [[CrossRef](#)] [[PubMed](#)]
25. Chiu, C.-P.; Solbrekken, G.L.; LeBonheur, V.; Xu, Y.E. Application of phase-change materials in Pentium (R) III and Pentium (R) III Xeon/supTM/processor cartridges. In Proceedings of the International Symposium on Advanced Packaging Materials Processes, Properties and Interfaces (IEEE Cat. No. 01TH8562), Braselton, GA, USA, 6–8 August 2002. [[CrossRef](#)]
26. Chiu, C.-P.; Chandran, B.; Mello, K.; Kelley, K. An accelerated reliability test method to predict thermal grease pumpout in flip-chip applications. In Proceedings of the 51st Electronic Components and Technology Conference (Cat. No. 01CH37220), Braselton, GA, USA, 29 May–1 June 2001; pp. 91–97. [[CrossRef](#)]
27. Akhtar, M.W.; Kim, J.S.; Memon, M.A.; Khan, M.Y.; Baloch, M.M. Surface modification of magnesium oxide/epoxy composites with significantly improved mechanical and thermal properties. *J. Mater. Sci. Mater. Electron.* **2021**, *32*, 15307–15316. [[CrossRef](#)]
28. Kemalolu, S.; Ozkoc, G.; Aytac, A. Properties of thermally conductive micro and nano size boron nitride reinforced silicon rubber composites. *Thermochim. Acta* **2010**, *499*, 40–47. [[CrossRef](#)]
29. Ramanathan, T.; Abdala, A.A.; Stankovich, S.; Dikin, D.A.; Herrera-Alonso, M.; Piner, R.D.; Adamson, D.H.; Schniepp, H.C.; Chen, X.; Ruoff, R.S.; et al. Functionalized graphene sheets for polymer nanocomposites. *Nat. Nanotechnol.* **2008**, *3*, 327–331. [[CrossRef](#)] [[PubMed](#)]
30. Akhtar, M.W.; Lee, Y.S.; Yoo, D.J.; Kim, J.S. Alumina-graphene hybrid filled epoxy composite: Quantitative validation and enhanced thermal conductivity. *Compos. Part B Eng.* **2017**, *131*, 184–195. [[CrossRef](#)]
31. Akhtar, M.W.; Memon, M.A.; Khan, M.Y.; Khalique, A.; Memon, A.G. Influence of Morphology and Surface Modification of MgO on Thermal Characteristics of Epoxy Composite. *ECS J. Solid State Sci. Technol.* **2021**, *10*, 087002. [[CrossRef](#)]
32. Gu, J.; Meng, X.; Tang, Y.; Li, Y.; Zhuang, Q.; Kong, J. Hexagonal boron nitride/polymethylvinyl siloxane rubber dielectric thermally conductive composites with ideal thermal stabilities. *Compos. Part A Appl. Sci. Manuf.* **2017**, *92*, 27–32. [[CrossRef](#)]
33. Talaei, Z.; Mahjoub, A.R.; Rashidi, A.; Amrollahi, A.; Meibodi, M.E. The effect of functionalized group concentration on the stability and thermal conductivity of carbon nanotube fluid as heat transfer media. *Int. Commun. Heat Mass Transf.* **2011**, *38*, 513–517. [[CrossRef](#)]
34. Guo, Y.; Wang, S.; Ruan, K.; Zhang, H.; Gu, J. Highly thermally conductive carbon nanotubes pillared exfoliated graphite/polyimide composites. *npj Flex. Electron.* **2021**, *5*, 16. [[CrossRef](#)]
35. Akhtar, M.W.; Lee, Y.S.; Yang, C.M.; Kim, J.S. Functionalization of mild oxidized graphene with O-phenylenediamine for highly thermally conductive and thermally stable epoxy composites. *RSC Adv.* **2016**, *6*, 100448–100458. [[CrossRef](#)]
36. Feng, Y.; Han, G.; Wang, B.; Zhou, X.; Ma, J.; Ye, Y.; Xie, X. Multiple synergistic effects of graphene-based hybrid and hexagonal boron nitride in enhancing thermal conductivity and flame retardancy of epoxy. *Chem. Eng. J.* **2020**, *379*, 122402. [[CrossRef](#)]
37. Shi, X.; Zhang, R.; Ruan, K.; Ma, T.; Guo, Y.; Gu, J. Improvement of thermal conductivities and simulation model for glass fabrics reinforced epoxy laminated composites via introducing hetero-structured BNN-30@BNNS fillers. *J. Mater. Sci. Technol.* **2021**, *82*, 239–249. [[CrossRef](#)]

38. Guan, C.; Qin, Y.; Wang, B.; Li, L.; Wang, M.; Lin, C.; He, X.; Nishimura, K.; Yu, J.; Yi, J.; et al. Highly thermally conductive polymer composites with barnacle-like nano-crystalline Diamond@Silicon carbide hybrid architecture. *Compos. Part B Eng.* **2020**, *198*, 108167. [[CrossRef](#)]
39. Peng, Y.; Liu, H. Effects of Oxidation by Hydrogen Peroxide on the Structures of Multiwalled Carbon Nanotubes. *Ind. Eng. Chem. Res.* **2006**, *45*, 6483–6488. [[CrossRef](#)]
40. Chen, D.; Zhu, L.; Zhang, H.; Xu, K.; Chen, M. Magnesium hydroxide nanoparticles with controlled morphologies via wet coprecipitation. *Mater. Chem. Phys.* **2008**, *109*, 224–229. [[CrossRef](#)]
41. Gao, G.; Pan, M.; Vecitis, C.D. Effect of the oxidation approach on carbon nanotube surface functional groups and electrooxidative filtration performance. *J. Mater. Chem. A* **2015**, *3*, 7575–7582. [[CrossRef](#)]
42. Figueiredo, J.L.; Pereira, M.F.R.; Freitas, M.M.A.; Órfão, J.J.M. Modification of the surface chemistry of activated carbons. *Carbon* **1999**, *37*, 1379–1389. [[CrossRef](#)]
43. Tuinstra, F.; Koenig, J.L. Raman Spectrum of Graphite. *J. Chem. Phys.* **1970**, *53*, 1126–1130. [[CrossRef](#)]
44. Eklund, P.; Holden, J.; Jishi, R. Vibrational modes of carbon nanotubes; Spectroscopy and theory. *Carbon* **1995**, *33*, 959–972. [[CrossRef](#)]
45. Ferrari, A.C.; Robertson, J. Interpretation of Raman spectra of disordered and amorphous carbon. *Phys. Rev. B* **2000**, *61*, 14095–14107. [[CrossRef](#)]
46. Scheibe, B.; Borowiak-Palen, E.; Kalenczuk, R.J. Oxidation and reduction of multiwalled carbon nanotubes—Preparation and characterization. *Mater. Charact.* **2010**, *61*, 185–191. [[CrossRef](#)]
47. Hou, P.-X.; Liu, C.; Cheng, H.-M. Purification of carbon nanotubes. *Carbon* **2008**, *46*, 2003–2025. [[CrossRef](#)]
48. Wepasnick, K.A.; Smith, B.A.; Schrote, K.E.; Wilson, H.K.; Diegelmann, S.R.; Fairbrother, D.H. Surface and structural characterization of multi-walled carbon nanotubes following different oxidative treatments. *Carbon* **2011**, *49*, 24–36. [[CrossRef](#)]
49. Datsyuk, V.; Kalyva, M.; Papagelis, K.; Parthenios, J.; Tasis, D.; Siokou, A.; Kallitsis, I.; Galiotis, C. Chemical oxidation of multiwalled carbon nanotubes. *Carbon* **2008**, *46*, 833–840. [[CrossRef](#)]
50. Min, S.; Blumm, J.; Lindemann, A. A new laser flash system for measurement of the thermophysical properties. *Thermochim. Acta* **2007**, *455*, 46–49. [[CrossRef](#)]
51. Zhao, Y.-H.; Wu, Z.-K.; Bai, S.-L. Thermal resistance measurement of 3D graphene foam/polymer composite by laser flash analysis. *Int. J. Heat Mass Transf.* **2016**, *101*, 470–475. [[CrossRef](#)]
52. Devpura, A.; Phelan, P.; Prasher, R. Percolation theory applied to the analysis of thermal interface materials in flip-chip technology. In Proceedings of the IThERM The Seventh Intersociety Conference on Thermal and Thermomechanical Phenomena in Electronic Systems (Cat. No. 00CH37069), Las Vegas, NV, USA, 23–26 May 2000.
53. Bokobza, L. Multiwall carbon nanotube elastomeric composites: A review. *Polymers* **2007**, *48*, 4907–4920. [[CrossRef](#)]
54. Wu, S.-Y.; Huang, Y.-L.; Ma, C.-C.M.; Yuen, S.-M.; Teng, C.-C.; Yang, S.-Y.; Twu, C.H. Mechanical, thermal and electrical properties of multi-walled carbon nanotube/aluminium nitride/polyetherimide nanocomposites. *Polym. Int.* **2012**, *61*, 1084–1093. [[CrossRef](#)]